

Modelling the Cloverleaf: Contribution of a Galaxy Cluster at $z \sim 1.7$. *

J.-P. Kneib¹ D. Alloin² Y. Mellier^{3,4,1} S. Guilloteau⁵ R. Barvainis⁶ R. Antonucci⁷

¹ Observatoire Midi-Pyrénées, CNRS-UMR5572, 14 Av. Edouard Belin, 31400 Toulouse, France

² CNRS-URA812, Service d'Astrophysique, CE Saclay, l'Orme des Merisiers. 91191 Gif-sur-Yvette Cedex, France

³ Institut d'Astrophysique, 98 bis Bd. Arago, 75014 Paris, France

⁴ Observatoire de Paris, DEMIRM, 61 Av. de l'Observatoire, 75014 Paris, France

⁵ Institut de Radio Astronomie Millimétrique, 300 rue de la Piscine, 38406 Saint Martin d'Hères, France

⁶ MIT Haystack Observatory, Westford, MA 01886, USA

⁷ UC Santa Barbara, Physics Department, Santa Barbara, CA 93106, USA

Received XXX, Accepted XXX

Abstract. We present a new investigation of the Cloverleaf ($z=2.558$) based on the combination of archival HST/WFPC2 data, recent IRAM CO(7-6) maps and wide field CFHT/FOCA2 images. The deepest WFPC2 observation (F814W) shows a significant overdensity of $I_{814W} \sim 23\text{--}25$ galaxies around the Cloverleaf that we interpret as the presence of a cluster of galaxies along the line of sight. The typical magnitude, red color ($R-I \sim 0.9$) and small angular size of these galaxies suggest that the cluster is very distant and could be associated with the absorption systems observed in the spectra of the quasar spots (either $z = 1.438, 1.66, 1.87$ or 2.07). The Cloverleaf is probably the result of the lensing effects of a system which includes, in addition to a single-galaxy, one of the most distant cluster of galaxies ever detected.

With this assumption, we have modelled the lens using altogether the HST/WFPC2 data and the IRAM/CO(7-6) map. We have considered two cases: one in which the mass model is a galaxy and a dark halo at $z=1.7$, and a second one in which the mass model is the combination of a cluster (centered on the overdensity of galaxies) and an individual galaxy located amid the Cloverleaf, both at $z=1.7$. The high-resolution IRAM/CO map provides for the first time the orientation and the ellipticity of the CO spots induced by the shear component. Velocity - positional effects are detected at a 8σ level in the CO map. A

strong limit can then be put on the size, shape and location of the CO source around the quasar. The CO source is found to form a ring-like structure orbiting the central engine at $\sim 100\text{km/s}$ at a radial distance of $\sim 100\text{pc}$, leading to a black-hole mass of $\sim 10^9 M_\odot$. The cluster component increases significantly the convergence of the lens and this pulls down the requirement on the mass of the lensing galaxy by a factor 2. This may explain the mystery of the lensing galaxy not detected yet. A deep high resolution infrared image should reveal the nature and location of the lensing galaxy.

The presence of an additional lensing cluster along the line of sight to the Cloverleaf strengthens the suspicion that many bright quasars are magnified by distant clusters of galaxies at redshifts larger than 1.

Key words: gravitational lensing - clusters of galaxies - gravitational lensing: Cloverleaf (H1413+117) - quasars : molecular content

1. Introduction

The Cloverleaf is the gravitationally lensed image of the distant quasar H1413+117 ($14^h 15^m 46^s.23 ; 11^\circ 29' 44''.0$ J2000.0) at $z = 2.558$ showing four spots with angular separations from $0''.77$ to $1''.36$. After its discovery (Magain et al. 1988), the Cloverleaf has been observed spectroscopically and imaged with ground based telescopes in various bands from B to I (Kayser et al 1990, hereafter K90, Angonin et al 1990, Arnould et al 1993) as well as at 3.6 cm with the VLA (K90). Models of the gravitational lens, involving one or two galaxies, were derived from these data sets, with some emphasis put on the VLA radio map (K90). However, the difficulty with these models lies in

Send offprint requests to: D. Alloin alloan@discovery.saclay.cea.fr

* Based on observations obtained at the Institut de Radio Astronomie Millimétrique, supported by INSU/CNRS (France), MPG (Germany), and IGN (Spain), at the Canada France Hawaii Telescope, supported by INSU/CNRS, the CNRC (Canada) and the University of Hawaii, and with the NASA/ESA Hubble Space Telescope, obtained from the data archive at the Space Telescope Institute. STScI is operated by the Association of Universities for Research in Astronomy, Inc. under the NASA contract NAS 5-26555.

the fact that they predict, for a $z=1.44$ lens, a mass of $\sim 2.5 \cdot 10^{11} h_{50}^{-1} M_\odot$ within $0.7''$ ($6 h_{50}^{-1}$ kpc) radius, which would correspond to a relatively bright normal galaxy: so far, searches in the K band of the predicted ‘bright’ lensing galaxies have been unsuccessful (Lawrence 1996) and this fact remains a mystery.

Except for a short report by Falco (1993) on the pre-COSTAR HST/WFPC observations of the Cloverleaf (used for the lens model derived by Yun et al (1997)), the post-COSTAR HST/WFPC2 data have not been fully exploited yet, though they may bring new constraints on the gravitational lens modeling.

New pieces of information also come from the detection of the Cloverleaf in the molecular CO transitions (Barvainis et al 1994, Wilner et al 1995, Barvainis et al 1997, Yun et al 1997, Alloin et al 1997). Both the physical conditions of the molecular gas in the quasar can be studied in detail (Barvainis et al 1997) and the gravitational lens model could be improved. Indeed, unveiling the gravitational lens nature of the Cloverleaf in CO (Alloin et al 1997) provides the true intensity ratios of the four spots, unaffected by absorption from intervening material, and unaffected by microlensing effects as the CO source in the quasar is not point-like (a gravitational shear is measured on the 3 brightest CO spots A, B & C). However, the different parts of the CO source suffering different amplification, the CO intensity ratios cannot be compared directly to the optical ones: this explains the corresponding observed differences reported by Alloin et al (1997). An improved CO(7-6) map, presented in this paper, has been obtained with the IRAM interferometer, giving further insight into the geometry of the quasar CO source.

In addition, CCD images of the Cloverleaf over a $5''$ field of view (CFHT/FOCAM archives) allow precise astrometry of the field and a better registration of the maps obtained through various wavebands, with a particular interest in the optical and the millimeter ones.

In the current paper, we take into account all these new constraints in order to derive an improved model of the gravitational lens and of the quasar molecular source. We present in Sect. 2 the new CO(7-6) data set and discuss in Sect. 3 the post-COSTAR HST/WFPC2 data, from the point of view of the Cloverleaf itself and of its environment. We provide in Sect. 4 the results of the astrometry performed from archived CFHT/FOCAM images and, using the CO(7-6) high resolution map obtained with the IRAM interferometer, we position very accurately the optical and millimeter data sets. A new gravitational lens model is computed and presented in Sect. 5, while the CO source in the quasar is discussed in Sect. 6. A final discussion and prospective analysis is given in Sect. 7. Throughout the paper, we use $H_0 = 50 h_{50}$ km/s/Mpc, $\Omega_0 = 1$ and $\Lambda = 0$.

2. IRAM Interferometric CO(7-6) improved map

Our previous CO(7-6) interferometer measurements (Alloin et al 1997) have been complemented with observations at intermediate baselines, performed on 1997 April 10 and 21 under excellent conditions. Calibrations were applied similarly to the previous data set. The combined data lead to the CLEANed integrated map restored with a $0.5''$ circular beam shown in Figure 1a. In order to search for a velocity gradient, we have first derived the spatially integrated line profile, following the procedure already discussed in Alloin et al (1997). The new CO(7-6) line profile, shown in Figure 2, exhibits a marked asymmetry with a steep rise on its blue side and a slower decrease on its red side. Excluding the central velocity channel, we have built the blue ($-225, -25$ km/s) and the red ($+25, +225$ km/s) maps displayed in Figures 1c and 1d respectively. The difference between the red-shifted and blue-shifted CLEANed maps (Figure 1b) establishes definitely the presence of a velocity gradient at a 8σ level. The implication of these results on the CO source will be discussed more thoroughly in Sect. 6.

Measurements of the spot characteristics from the CO(7-6) image have been performed (spot flux ratios, sizes and orientations) through a fitting procedure in the visibility domain, as explained in Alloin et al (1997). The final parameters are provided in Table 1 where the spot sizes are intrinsic to the image, *i.e.* deconvolved by the interferometer beam. Although the measurements have not been corrected for seeing effects (mean seeing estimate of the order of $0.2''$) the spots A, B and C appear to be definitely elongated (see Figure 3 for spot labels).

3. HST/WFPC2 observations

3.1. The HST/WFPC2 data set

The HST data of the Cloverleaf used in this analysis have been provided by the ESO/ST-ECF Science Archive Facility (Garching). Two data sets obtained with the WFPC2 are presented here. The first one was obtained by Turnshek (1994 July 12 [ID:5442] & 1994 December 23 [ID:5621]) and the second one by Westphal (1995 April 27 [ID:5772]). Turnshek’s observations aimed at discovering the lensing galaxy. They consist in WFPC-2 images and FOS spectra of the four quasar images and of the suspected lensing object. These observations were not successful in finding the lensing galaxy, but the FOS spectra of the four quasar spots have been discussed by Turnshek (1996). Observations of the Cloverleaf by Westphal are part of a larger programme to study multiple quasars and their environments. Standard reduction procedures using IRAF/STSDAS packages have been applied. The absolute photometry was obtained using magnitude zero-points given in Holtzmann et al. (1995). Information about the final images in filter

Fig. 1. Image of the Cloverleaf obtained with the IRAM telescope at Plateau de Bure. (a) is the total CLEANed image, (c) the CLEANed blue-shifted image, (d) the CLEANed red-shifted image and (b) the difference between the CLEANed red and CLEANed blue image. The CLEANed CO(7-6) maps were obtained with a natural beam of $0.8'' \times 0.4''$ at P.A. 15 deg. They have been restored with a circular $0.5''$ beam for comparison with HST data. Contour spacing is 1.35 mJy/beam for 1a, 2 mJy/beam for 1c and 1d and 3 mJy/beam for 1b, corresponding in each case to 2σ .

Spot	$\Delta\alpha$ ('')	$\Delta\delta$ ('')	Flux (mJy)	Major axis ('')	Minor axis ('')	P.A.
Velocity Range -225, +225 km/s						
A	0	0	12.9 (2.1)	0.50 (0.17)	0.30 (0.14)	0 (23)
B	0.71 (0.026)	0.15 (0.033)	26.7 (1.9)	0.60 (0.08)	0.25 (0.12)	70 (12)
C	-0.38 (0.018)	0.63 (0.023)	24.0 (2.0)	0.66 (0.10)	0.40 (0.08)	-3 (8)
D	0.42 (0.025)	1.02 (0.030)	17.0 (1.9)	0.56 (0.11)	0.25 (0.20)	73 (15)
Velocity Range -225, -25 km/s						
A	0	0	13.5 (2.2)	0.49 (0.24)	0.30	0
B	0.71	0.15	24.4 (2.2)	0.48 (0.10)	0.25	70
C	-0.33 (0.02)	0.56 (0.03)	30.8 (2.1)	0.60 (0.11)	0.40	0
D	0.42	1.02	14.9 (2.3)	0.30 (0.16)	0.25	75
Velocity Range +25, +225 km/s						
A	0	0	10.8 (2.2)	0.32 (0.33)	0.30	0
B	0.71	0.15	27.4 (2.2)	0.63 (0.08)	0.25	70
C	-0.41 (0.02)	0.69 (0.03)	19.1 (2.1)	0.52 (0.16)	0.40	33 (25)
D	-0.29	0.87	18.3 (2.3)	0.60 (0.15)	0.25	75

Table 1. The Cloverleaf CO(7-6) image: positional shifts, fluxes and elongations of the spots. One σ error bars are given within brackets. When no error bar is given, the value was fixed from the fit to the -225,225 km/s image.

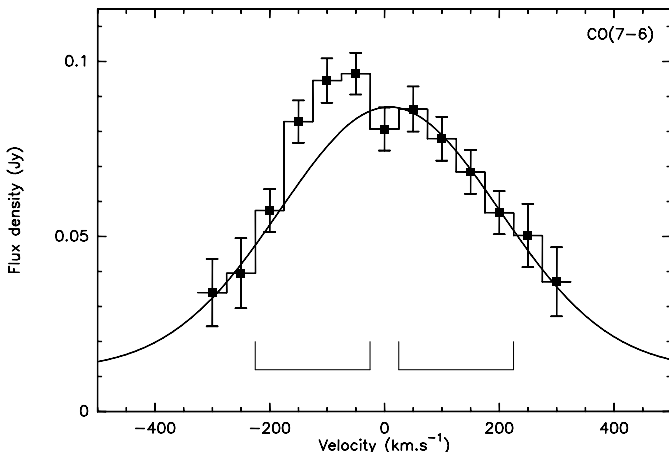


Fig. 2. Spectrum of the CO(7-6) line towards the Cloverleaf. Error bars are $\pm 1\sigma$. The thin line corresponds to the best gaussian fit to the wings and the red side with FWHM ~ 450 km/s, although it is obvious that the line profile differs from a smooth gaussian shape and shows an excess of emission on its blue side. The offset of the baseline from zero corresponds to 13 mJy of continuum flux; this is larger than the 5 ± 3 mJy reported by Alloin et al (1997), owing the inclusion of shorter baselines in the new dataset and detection of a more extended continuum component. The central frequency is 226.715 Ghz.

F336W (central rest wavelength ~ 945 Å), F555W (central rest wavelength ~ 1560 Å), F702W (central rest wavelength ~ 1975 Å), and F814W (central rest wavelength ~ 2290 Å) are summarized in Table 2.

3.2. Properties of the Cloverleaf images

Two types of information are relevant for our present goal of modelling the gravitational lens : the relative astrometry (with respect to spot A, as shown on Figure 3) as well as the shape of the four spots and their intensity ratios.

Regarding the relative astrometry and spot sizes, the PC observations in filters F336W, F555W, F702W and F814W provide similar results displayed in Table 3. The four spots are stellar-like with a FWHM ≈ 1.5 pixel or $0.068''$.

The absolute photometry and the relative intensity ratios (Table 4) have been computed with the Sextractor software (Bertin & Arnouts 1996) using total and isophotal magnitudes when images of the quasar were not saturated. No PSF fitting was applied as the four different spots are well separated on the PC; furthermore a PSF fitting would not have been possible for the December 1994 data as the PSF was not circular for this observation (see caption of Table 2). The important variation of the intensity ratios in U compared to V, R and I band could probably be only explained by absorption along the line of sight by intervening galaxies (H α clouds at redshift ~ 1.7

Date YY/MM/DD	Integration time seconds	Filter	QSO location	Wavelength range (rest frame) Å	contributor	comments
94/07/12	2400	F255W	PC1	646–843	below Lyman limit	No detection
94/07/12	200	F702W	PC1	1686–2360	Cont. + CIII]	OK
94/07/12	2700	F702W	PC1	1686–2360	Cont. + CIII]	quasar saturated
94/12/23	2700	F336W	PC1	871–984	Continuum	PSF not circular
94/12/23	400	F702W	PC1	1686–2360	Cont. + CIII]	PSF not circular
94/12/23	900	F814W	PC1	1967–2726	Cont.	PSF not circular
95/04/27	23	F555W	PC1	1264–1826	Cont. + CIV	short exposure
95/04/27	60	F814W	PC1	1967–2726	Cont.	short exposure
95/04/27	2800	F814W	WF3	1967–2726	Cont.	quasar in WF3 chip

Table 2. Summary of the HST data sets. Note: the data set of 1994 December shows a weird PSF, though the FGS status was on the FINE guiding mode: it may be due to some guiding problem resulting from the paucity of guide stars in this area.

Spot	α (J2000)	δ (J2000)	$\Delta\alpha$ (arcsec)	$\Delta\delta$ (arcsec)
A	14 15 46.21	11 29 42.75	0.	0.
B	14 15 46.26	11 29 42.92	$+0.75 \pm 0.01$	$+0.17 \pm 0.01$
C	14 15 45.18	11 29 43.48	-0.49 ± 0.01	$+0.73 \pm 0.01$
D	14 15 46.23	11 29 43.79	$+0.36 \pm 0.01$	$+1.04 \pm 0.01$

Table 3. Absolute and relative astrometry of the four quasar spots. The absolute position of the brightest spot A comes from CFHT/FOCAM images (coordinates are given within a 0.15" rms accuracy), while the relative positions of B, C and D with respect to A are from the WFPC2/PC1 data.

will act as very efficient absorbers in the U band). This absorption has to be larger for the spots A & B which display the biggest relative change to the C & D spots. No obvious evidences of microlensing are detected from the HST data set, though small variations in the quasar spot intensity ratios are consistent with the ESO/NOT monitoring of the Cloverleaf (Østensen et al 1997).

3.3. The Cloverleaf environment

Figure 4 shows the deep F814W image of the Cloverleaf. The four quasar spots lay at the center of the WF3 chip. The presence of numerous faint objects in the environment of the Cloverleaf is striking over a 40" region. In order to quantify this effect we have computed the object number density, $\langle N \rangle$, and its dispersion, σ_N , in the magnitude range $I=23$ to 25. We have estimated this density in different regions across the image: in a 40" diameter region around the Cloverleaf where the density contrast is clearly visible by eye and in various randomly selected areas of similar size. On the whole frame we find a mean value $\langle N \rangle_{whole} = 45 \pm 20$ objects/arcmin² (1 σ). The region around the Cloverleaf has $\langle N \rangle_{Cl} = 85 \pm 30$ objects/arcmin², with a peak at 130 objects/arcmin². The detection of a peak is therefore significant at a 4 σ level. This brings us to suspect the presence of a cluster of galaxies (of unknown redshift), which could contribute significantly to the gravitational lens effect. We provide in Figure 5 the deep F702W image of the Cloverleaf where the four quasar spots lay at the center of the PC1 chip. Similarly to the F814W image we have plotted the number

density isocontours of faint objects between $R=23$ to 25. There is no overdensity larger than 2 σ . Therefore, we conclude that the 4 σ overdensity around the Cloverleaf is significant. Fig. 6 shows a zoom of this area from the deep F814W image: the photometry and color of the related objects (obtained by combining WF and PC observations) are given in Table 5. The bulk of them are red objects with $R_{702W} - I_{814W} \sim 0.9$ (from 0.7 to 1.2). While their morphology cannot be obtained from the HST images, their red color suggest that we might be dealing with E/S0 galaxies in a high-redshift cluster.

The small size (of the order of 0.3" which hampers any strong morphological classification), faint magnitude ($23 < I$) and red color $R_{702W} - I_{814W} \sim 0.9$ of these galaxies are suggestive of *high-redshift* E/S0 galaxies (as can be found for example in the CFRS sub-sample of galaxies with $1 < z < 2$ (Lilly et al 1995)). Moreover, the significant *concentration* of these galaxies near the particular line of sight to the multiple quasar is a convincing indicator of the presence of a *high-redshift cluster*. This cluster could either be linked physically to the quasar at redshift $z \sim 2.56$ or along the line of sight. Hereafter, we *assume* this cluster to be at a redshift close to that of the narrow absorption systems observed by Turnshek et al (1988), and Magain et al (1988): either 1.438, 1.661, 1.87 or 2.07. For the sake of simplicity, we shall adopt hereafter a value of 1.7. Since no observations are available yet in the near infrared, it is practically impossible to obtain secure photometric redshifts in this redshift range (*e.g.* the 4000 Å break would fall at $1\mu\text{m}$ at $z=1.7$). Dedicated high-resolution IR imaging and/or optical/IR spectroscopy should be carried on

Date	U _{336W} [ratio]	V _{555W} [ratio]	R _{702W} [ratio]	R _{702W} [ratio]	I _{814W} [ratio]	I _{814W} [ratio]
	94/12/23	95/04/27	94/07/12	94/12/23	94/12/23	95/04/27
A	18.95 [1.00]	18.02 [1.00]	17.71 [1.00]	17.68 [1.00]	17.45 [1.00]	17.35 [1.00]
B	19.31 [0.73 ± 0.01]	18.19 [0.86 ± 0.01]	17.90 [0.85 ± 0.01]	17.82 [0.88 ± 0.01]	17.58 [0.89 ± 0.01]	17.47 [0.89 ± 0.01]
C	18.93 [1.01 ± 0.01]	18.25 [0.81 ± 0.01]	18.02 [0.76 ± 0.01]	17.95 [0.77 ± 0.01]	17.73 [0.76 ± 0.01]	17.66 [0.76 ± 0.01]
D	19.13 [0.85 ± 0.01]	18.36 [0.75 ± 0.02]	18.12 [0.69 ± 0.01]	17.97 [0.74 ± 0.01]	17.81 [0.70 ± 0.01]	17.73 [0.69 ± 0.01]
	B (K90)	R (Magain et al)	R (K90)	R (Angonin et al)	I (K90)	
Date	88/04/27	88/03/08	88/04/27	89/03/07	88/04/27	
A	[1.00]	[1.00]	[1.00]	[1.00]	[1.00]	
B	[0.84]	[0.87]	[0.85]	[0.88 ± 0.02]	[0.90]	
C	[0.83]	[0.76]	[0.74]	[0.78 ± 0.02]	[0.76]	
D	[0.61]	[0.69]	[0.61]	[0.66 ± 0.02]	[0.59]	

Table 4. Total magnitude and relative intensity ratios of the four quasar spots from the WFPC2/PC1 data, compared to previous observations found in the literature.

Fig. 4. Image of the whole HST field around the Cloverleaf obtained with the WFPC2 camera. The four quasar spots are not resolved in this figure but are located at the center of the WF3 chip (bottom-right). The galaxies detected in the field by the SExtractor software (Bertin & Arnouts 1996) are overlayed with elliptical contours indicating their centroid, orientation and ellipticity. The white contours are iso-number density of galaxies with $23 < I < 25$ (ranging from 30 to 80 galaxies/arcmin 2). A significant density enhancement is clearly visible around the Cloverleaf, and is found to be almost centered on the 4 quasar spots. This is a good indication that a distant cluster of galaxies lies on the line of sight to the Cloverleaf: the presence of this cluster certainly increases the convergence of the lensing galaxy.

Fig. 5. F702W mosaic image of the field around the Cloverleaf. The four-spot quasar is located at the center of the PC chip. Same convention as in Figure 4. The white contours are iso-number densities of galaxies with $23 < R < 25$ ranging from 30 to 60 galaxies/arcmin 2 .

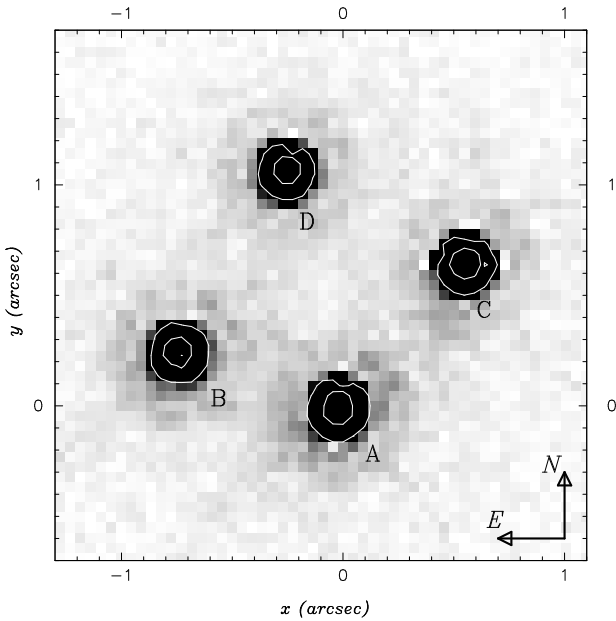


Fig. 3. Image of the Cloverleaf obtained with the HST/WFPC2 through the F702W filter (central rest wavelength ~ 1975 Å). The spots shape is perfectly circular. The spots are labelled A, B, C, D, following Magain et al (1988).

Fig. 6. Zoom of the deep F814W image of the Cloverleaf (rotated to be in RA-DEC coordinate system: x-axis is $-\alpha$, y-axis is $+\delta$). The galaxies with $22.5 < I < 25$ detected in the field by the SExtractor software (Bertin & Arnouts 1996) are overlayed with elliptical contours indicating their centroid, orientation and ellipticity. Photometry and color of these galaxies are provided in Table 5. The dashed square overlaid corresponds to the location of the PC R_{F702W} image. The cross correspond to the center chosen for the cluster mass component (model 2).

the objects forming this overdensity in order to determine their distance and nature.

We have examined the alternative possibility that this ensemble of faint sources corresponds to a population of HII regions in a nearby galaxy with low surface brightness, extending over 40" in diameter. The intrinsic size of such a dwarf galactic system, around 10 kpc, requires that its distance should be less than 50 Mpc (or its redshift less than 0.01). However, the observed R-I ~ 0.9 color of the objects forming the overdensity, is far too red to fit the R-I color of giant extragalactic HII regions observed in a sample of nearby HII galaxies, R-I ~ -0.17 (Telles et al 1997) or as modelled, R-I ~ -0.2 (e.g. Bica et al 1990). Furthermore, the observed I magnitudes are too large by at least

ID Number	$\Delta\alpha$ (arcsec)	$\Delta\delta$ (arcsec)	I_{814W}	$R_{702W} - I_{814W}$
1	-4.7	-6.2	22.52	0.72
2	-5.6	-3.9	23.11	0.86
3	7.3	-3.7	23.16	0.88
4	13.2	8.7	23.57	0.59
5	-13.7	16.2	23.61	1.01
6	7.2	13.8	23.73	0.94
7	-3.9	5.4	23.75	0.74
8	-4.3	0.6	23.78	1.16
9	0.1	-5.8	23.94	0.12
10	-14.7	9.1	23.95	1.09
11	-5.4	5.3	24.01	1.09
12	-14.2	-2.4	24.20	0.43
13	8.0	-11.6	24.20	0.92
14	1.7	4.2	24.37	> 1.1
15	-8.2	0.6	24.41	1.05
16	11.4	-6.7	24.55	> 0.9
17	3.4	0.1	24.62	> 0.9
18	-7.2	14.4	24.66	0.91
19	4.5	-2.9	24.74	0.88
20	-8.1	-3.6	24.78	> 0.7
21	-2.7	-14.4	24.80	> 0.7
22	-9.7	12.9	24.84	> 0.7
23	2.2	-9.1	24.89	> 0.6
24	12.0	0.3	24.93	0.13

Table 5. Relative position from the quasar spot A, total magnitude and color of the galaxies detected in I_{F814W} (numbered as in Figure 6). Typical error for the faintest object is 0.2 mag.

7 magnitudes with respect to expected values of such an HII population located in the local Universe. Therefore, this interpretation should be discarded.

3.4. The lensing object

Although the cluster candidate mentioned earlier is acting as an additional lensing agent, the small angular separation between the four spots implies that most of the lensing effect is likely produced by a galaxy located amid the four spots of the quasar. This lensing galaxy has not been detected so far on “deep” visible and near infrared ground based observations (Angonin et al 1990; Lawrence 1996).

Yet, the detection of the lensing galaxy would be of great importance to model accurately the mass distribution of the lens as we could then assume that the mass follows the geometry of the light, as in other successful lensing model calculations and as expected in the inner regions of galaxies.

We tentatively used the deepest WFPC2/F814W images in order to detect the central lensing galaxy. The four spots of the quasar have been subtracted using the PSF model provided by the nearby star. Due to the significant light residual related to the quasar photon noise, the tele-

scope diffusion and the first diffraction rings, the limiting surface brightness in the center of the Cloverleaf is at least 1 mag lower than across the whole image. This reduces the limiting magnitude to a value of $I \sim 24$, though the faintest objects detected in the field have $I \sim 25$. Even at such a faint magnitude, there is no evidence of a signal spread over few pixels. We conclude that the lensing galaxy must have $I > 24$. We can set an upper limit on its velocity dispersion, assuming the extreme case where the lens is an elliptical galaxy fainter than $I=24$ with a redshift close to that of the narrow absorption lines seen on the quasar spectrum at $z \sim 1.7$. In order to infer the absolute magnitude of the corresponding lens, we have run a galaxy evolution model for an elliptical galaxy with standard parameters (power law Initial Mass Function with one segment ranging from 0.1 to $125 M_{\odot}$, single burst of star formation, $\Omega=1$, $H_0=50$ km/sec/Mpc) from Bruzual & Charlot (1993). We find that in the most favorable case, the galaxy should have an absolute magnitude larger than $M = -21.3$ in order not to be detected. Using the Faber-Jackson relation (Fall 1981), we derive an upper limit of its velocity dispersion $\sigma = 350$ km/sec. A similar study can be performed using the 2000 sec. K-band exposure obtained at Keck (Lawrence 1996). Given the expected throughput of the Keck camera, we estimate the central lensing galaxy to have $K > 22$, which is a constraint not as stringent as that derived from the HST images. Hence, the visible and near infrared data are not sufficient to constrain the mass of the lensing galaxy. But in fact, if we take into account the likely presence of the distant cluster, it is no longer necessary to invoke a large mass (i.e. high brightness) for the lensing galaxy since a fraction of the convergence and the deflection angle would be contributed by the cluster.

4. Additional constraints from the absolute registration of images in various wavebands

In order to derive precisely the shear induced by the gravitational lens on an extended source in the quasar, it is imperative to register with a high accuracy the Cloverleaf image in a waveband corresponding to point-like images of the quasar (i.e. R-band corresponding to rest wavelength 1967 Å) and in a waveband corresponding to an extended source in the quasar (i.e. the CO(7-6) molecular emission). The high precision requested, better than 0.2”, cannot be achieved from the HST data because of their limited field of view. Hence, we have searched for wide-field exposures of the Cloverleaf field obtained under good seeing conditions at CFHT.

4.1. The FOCAM CFHT data set

We have retrieved from the CFHT data archive (CADC database in Victoria) three images obtained on 1992 February 27 by Angonin, Vanderriest and Chatzichristou, with

FOCAM. The CCD in use was Lick II (1500 pixels of 0.2''), covering a 5' field. Two images were obtained through the R band and one through the I band, under a 0.6'' seeing condition. For every image, the integration time was 310 seconds. To derive the astrometry, we used the two R band direct images, unprocessed since we are only interested in the astrometric information.

4.2. Absolute astrometry

The absolute astrometry was performed using 6 reference stars across the field, from the Cambridge APM database. This allows absolute positioning of the brightest spot A within an accuracy of 0.15'' (rms). Then, we have used the relative astrometry of spots B, C and D, with respect to A, from the HST image (relative accuracy $\pm 0.01''$). The absolute astrometry of the Cloverleaf is provided in Table 3 (J2000.0).

4.3. Registration of the optical and millimeter images

The IRAM CO(7-6) image is obtained within an absolute astrometric accuracy of 0.1'' (rms), quite comparable to that achieved from the combined CFHT/FOCAM and HST/WFPC2 results. Therefore, it is possible to register both the optical and the millimeter data in an absolute manner (Figure 1). This is the starting point of our new modelling of the Cloverleaf.

In summary, we consider for the modelling the positions as well as R and I intensity ratios of the four spots given in Table 4, since we know that they are not affected by any spatial resolution effect. Conversely, the relative positions of the CO spots with respect to the visible spots are subject to some spatial resolution effect because the interferometer natural beam size is of the order of the spot size. Therefore, we shall not use the CO spot positions to build the lens model, but rather check whether the CO spots predicted by the lens model and convolved by the interferometer beam reproduce the observed offsets between the CO and the visible spots (see Sect. 5 and 6)

5. New model of the Cloverleaf gravitational lens

5.1. The procedure

The modelling of the Cloverleaf is based on the minimization algorithm described previously in several papers (Kneib et al 1994, 1996) and used to model giant arcs in lensing clusters. This algorithm adjusts the parameters of the model through a minimization of the differences in the position and the geometry of the lensed spots once they are sent back to the source plane. The fitting uses observational constraints like the position, intensity and shape of the lensed spots and eventually the light distribution

associated with the deflector as additional information on the mass distribution. The model incorporates parameters of the lensing potential, through a simple analytical representation of the mass distribution. In the present case, we use the difference of two pseudo-isothermal elliptical models (PIEMD) (Kassiola & Kovner 1993, Hjorth & Kneib 1997):

$$\Sigma(R) = \Sigma_0 \frac{as}{s-a} \left(\frac{1}{\sqrt{a^2 + R^2}} - \frac{1}{\sqrt{s^2 + R^2}} \right) \quad (1)$$

where a is the core radius and s is the truncature radius. Moreover we have $R^2 = (x-x_0)^2/(1-\varepsilon) + (y-y_0)^2/(1+\varepsilon)$, where (x_0, y_0) are the centre position, (x, y) the current position in the principal axis of the lens, and $\varepsilon = (a^2 - b^2)/(a^2 + b^2)$ is the ellipticity of the mass distribution. The important characteristic of such a model is that the mass distribution has an elliptical symmetry whatever ε . Its $1/R^3$ dependency at large radii imposes a finite mass to the model, and is compatible with the theoretical prescription of violent relaxation models (Hjorth & Madsen 1991). Furthermore, the model treatment is fully analytical.

The constraints used for the gravitational lens modelling are as follows:

1. the *relative positions* of the quasar spots from the HST and the *intensity ratio* taken in the R and I band. These constraints will primarily enable us to determine the mass model.
2. the *non-detection* of a 5th spot, which puts a limit on the size of the lens core.
3. the *position of the cluster center* as measured from the overdensity of galaxies near the Cloverleaf.
4. both the cluster and the lensing galaxy are assumed (for convenience) to be at $z=1.7$.

The *relative intensity ratios* and the measured shapes of the CO spots are used as a test of the model, and provide as well information on the size and geometry of the CO source.

5.2. Results

We have computed two types of model: model 1 which includes an individual galaxy with a dark halo at $z=1.7$ and model 2 which considers an individual galaxy and a cluster both at $z=1.7$. These model are not unique but give similar qualitative results. The parameters for the lensing galaxy and the cluster component are shown in Table 6. The cluster component is poorly known since we were not able to derive significant constraints on the lensing galaxy from the photometry (see Sect. 3.3). Yet, once an upper limit has been found for the velocity dispersion of the lensing galaxy, any model including an additional lens-plane (such as that of the galaxy cluster) and implying a mass, hence a velocity dispersion for the individual

Positions	Galaxy ($z = 1.7$)	Dark Halo ($z = 1.7$)
$\Delta\alpha$	0.187 ± 0.01	0.187
$\Delta\delta$	0.563 ± 0.01	0.563
$a (h_{50}^{-1} \text{ kpc})$	0.05 (fixed)	4.4 ± 1
$s (h_{50}^{-1} \text{ kpc})$	20.0 ± 5	250 ± 20
PA	$21.5^\circ \pm 3$	21.5°
ε	0.1 ± 0.05	0.2 ± 0.1
σ (km/sec.)	127 ± 10	395 ± 20

Positions	Galaxy ($z = 1.7$)	Cluster ($z = 1.7$)
$\Delta\alpha$	0.174 ± 0.01	4.7 (fixed)
$\Delta\delta$	0.548 ± 0.01	-6.2 (fixed)
$a (h_{50}^{-1} \text{ kpc})$	0.05 (fixed)	50 ± 10
$s (h_{50}^{-1} \text{ kpc})$	$30. \pm 5$	700 (fixed)
PA	$-32^\circ \pm 2$	-30 ± 5
ε	0.33 ± 0.05	0.2 ± 0.1
σ (km/sec.)	230 ± 10	1100 ± 100

Table 6. Results of the lens modelling of the Cloverleaf. The first model does not include a cluster component, while the second one does.

lensing galaxy lower than this limit, is formally acceptable, provided the gravitational shear observed on the CO map is modelled equally well.

To test, at first order, the lens model with the CO(7-6) map, we have assumed the CO source to be elliptical with a gaussian profile. We have fitted position, size and ellipticity so that it reproduces the observed CO image. The upper limit of its size is provided by the CO elongated spots A and B which are close to merging, but still clearly separable. Thus, the model must predict, in the image plane, disconnected isocontours of the A and B spots. However, we underline that this estimated size also depends on the ellipticity of the lens mass distribution (as the scale in the source is proportional to εR_E where R_E is the Einstein radius). We found for model 1 a typical size of 460×230 pc (FWHM) for model 1, and 155×110 pc (FWHM) for model 2. In the present case, 1" in the source plane translates into 7.68 kpc in the chosen cosmology. A summary of the CO modeling is displayed in Figure 7. Figure 7j shows the CO emission of Figure 7b before convolving it by the interferometer natural beam. It clearly shows us that it will be difficult to reach a higher degree of precision in describing exactly the source morphology, unless higher-resolution CO images can be acquired. An additional effect of the convolution results in an apparent shift of the centroids of the CO spots with respect to the quasar point-like spots. This demonstrates that the displacements observed between the centroids of the CO and visible spots are artifacts of the distorted morphology of the CO emission in the image plane.

The amplification ratios inferred from the modelling and the observations are displayed in Table 7. The agreement between the expected amplifications and the observed flux ratios is relatively good. The quasar intrinsic magnitude is about $I \sim 20.5$. The comparison between the expected amplification and the observed ones in CO is not easy.

Differential amplification due to the CO source extent and location with respect to the diamond caustic can explain the observed difference. The total amplification of the CO emission is ~ 18 for model 1 and ~ 30 for model 2.

5.3. Comparison with previous models

The comparison with previous models presented by K90 and recently by Yun et al (1997) is somewhat difficult. First, none of these included a lensing contribution from a distant galaxy cluster. Regarding the properties of the individual lensing galaxy, the K90 model 1 (see Table 4 and Figure 4a of K90) is close to our results. The relative position of the source and the lensing galaxy center are almost identical and the orientation of the gravitational potential is similar (70° instead of 80°). The upper limit on the velocity dispersion we find when no cluster component is introduced is 280 km/s, in excellent agreement with their upper limit (< 285 km/sec). But on the other hand, our ellipticity is significantly different. Assuming K90 used the standard definition of the eccentricity ($e = \sqrt{1 - b^2/a^2}$) for the projected mass density, the corresponding ellipticity is $\varepsilon = 0.688$, which is 3.5 times larger than in our results. This difference results from the analytical form of the mass profile chosen: K90 used a Singular Isothermal Sphere (SIS) while we are using a truncated PIEMD with two parameters for the shape of the profile. Then, more freedom is given in the radial mass profile, leading to solutions with smaller ellipticities (cf. the model of H14176 in Hjorth & Kneib 1997).

On the contrary, our results do not agree with those by Yun et al (1997) who find a lensing elliptical potential perpendicular to that derived by K90 and to ours. Indeed, the four CO spots observed (and predicted by our lens model) better constrain the orientation of the potential (although they do not insure the uniqueness of the solution).

6. Constraints on the quasar CO source

In addition to the size of the quasar CO source, ~ 460 pc FWHM, as derived above (see Sect. 5.2), we can obtain some information on its substructure using the velocity gradient observed in the CO(7-6) line (Figure 1b). Indeed, the map (Figure 1c) corresponding to the blue side of the line (-225,-25 km/s) shows that spot C is stronger and slightly displaced inwards with respect to its counterpart in the map corresponding to the (+25,+225 km/s), shown in (Figure 1d). A hint of this effect can be found in Yun et al (1997) although a close comparison of the IRAM results with the OVRO one is hampered by the fact that in their study the spatial resolution is twice lower, the line profile is not shown, the velocity interval considered -145 km/s is narrower than ours - 200 km/s - and not positioned precisely with respect to the line center.

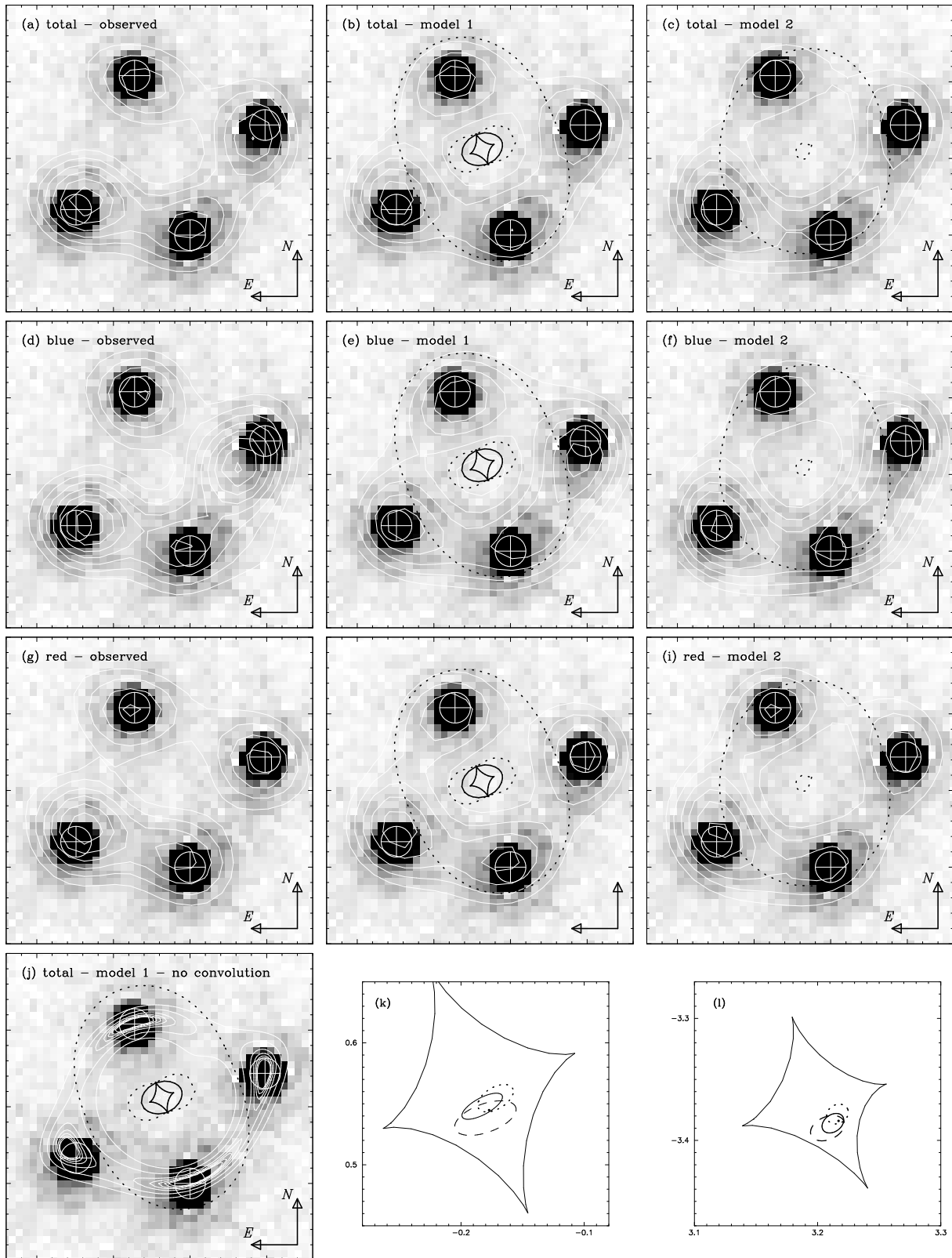


Fig. 7. Results of the lens modelling of the Cloverleaf superimposed on the HST image. (a) is the HST image overlaid with the CO observed (-225, +225 km/s); (b) is the CO predicted for model 1, convolved by the interferometer beam. (c) is similar as (b) but for model 2. (j) is the the CO predicted for model 1, not convolved by the interferometer beam. (d), (e), (f) is similar as the first line but for the blue emission. (g), (h), (i) is similar as the first line but for the red emission. The dotted line is the corresponding critical line. (k) gives the position of the best fitted sources for the blue (dashed), red (dotted) and total (solid) emission, for model 1. (l) is similar as (k) but for model 2. The central diamond-shape curve (in (b), (e), (h), (k) and (l)) is the internal caustic crossed by the lensed CO source at redshift $z=2.558$.

Spot	Lens model 1	Lens model 2	HST (visible)	IRAM (CO)
A	[2.99] 1.0	[3.16] 1.0	1.0	1.0
B	[2.84] 0.87	[3.36] 1.20	0.88 ± 0.01	2.07 ± 0.48
C	[2.80] 0.84	[2.93] 0.81	0.76 ± 0.01	1.86 ± 0.45
D	[2.66] 0.74	[2.71] 0.66	0.71 ± 0.01	1.32 ± 0.36
E	[-4.88] 0.0007	[-7.45] 5e-5	-	-

Table 7. Amplification ratios of the four spots as inferred from the lens modelling and compared with the visible and the CO (-225,+225 km/s) flux ratios. For the model we also give the δm amplification within brackets. Accounting for the errors, the model reproduces the amplification ratios reasonably well. The last line gives the amplification ratio of the fifth spot. It is considerably demagnified. Since it is not detected on the visible data, we expect its magnitude to be fainter than $m_I = 25$., which implies that the quasar itself is fainter than $m_I = 16.6$.

Therefore, we shall concentrate now on the interpretation of the IRAM data set only. Using the two lens models obtained in Sect. 5.2, we optimized the structure of the CO source to reproduce separately the red and the blue images (Figure 7). We call attention to the fact that a precise registration (better than 0.1'') of the CO map and the HST data is required to achieve a detailed structure of the CO source.

For model 1 [resp. model 2], we find an offset of 0.03'' (~ 230 pc) [resp. 0.02'' (~ 150 pc)] between the center of regions emitting the blue and red parts of the CO line (c.f. Figure 7). We have tested this procedure against uncertainties in the CO/HST images registration. A change by 0.05'' (half a CO map pixel) has very minor impact on the positions of the source regions emitting the blue and red parts of the line. The quasar point-like visible source appears to be almost exactly centered between the blue- and red-emitting regions. This is reminiscent of a ring-like structure orbiting the quasar at the radius of ~ 100 pc [resp. 75 pc] and with a Keplerian velocity of ~ 100 km/s (assuming a 90 deg inclination with respect to the plane of the sky), the resulting central mass would be $\sim 10^9 M_\odot$ [resp. $\sim 7.5 \cdot 10^8 M_\odot$]. Elaborating a more sophisticated (realistic) model of the CO source and its link with the BAL feature also observed in this quasar is beyond the current analysis but should be performed in the future. Regarding the spot fluxes in CO(7-6) as derived from the maps in Figures 1a, 1c, 1d and Table 1, a comparison with the fluxes given previously in Alloin et al (1997) is not straightforward because the velocity interval over which the integration has been performed is different in the two studies (-225,+225 km/s vs. -325,325 km/s). The amplification factor being extremely sensitive to the position of the emitting region with respect to the caustic, any velocity-positional changes within the source can result in a different configuration in the image plane. Such gradients are likely to occur in the molecular torus of the standard AGN model. The differential amplification resulting from this gradient is probably at the origin of the asymmetry observed in the line profile (Figure 2).

7. Discussion, Prospective and Conclusion

The complete multi-wavelength analysis of the Cloverleaf reveals that this is probably a complex lens which includes a lensing galaxy and an additional distant lensing cluster of galaxies. The reality of the cluster toward the Cloverleaf has still to be confirmed independently. Even at the level of a 4σ detection, clustering and projection effects can not be readily discarded to explain the observed galaxy enhancement, and measuring the redshift of these galaxies is of high priority to position them in the redshift space.

Yet, most of the galaxies around the Cloverleaf are found in the same magnitude and size ranges, as expected if they indeed belonged to a cluster. If the cluster is at a very large distance, the shift of its galaxy luminosity function up to higher apparent magnitude would explain why the number-density contrast of the cluster with respect to faint field galaxies is lowered down to only a 4σ level.

This interpretation implies that the lensing galaxy may not be very massive and consequently may not be very luminous, which would explain the mystery of the lensing galaxy not having been detected so far. The drawback is that, despite the constraint that the shapes of the CO spots provide on the orientation of the mass density distribution, it mandates sharing the mass between the lensing-galaxy and the lensing-cluster which increases the number of possible lens configurations. Hence, it considerably reduces the chances to infer a secure measure of the Hubble constant from the time delay measurements of lightcurves between the four spots (a thorough report of the variability of the quasar is given in Østensen et al. 1997). Thus, we need to confirm, probably from ultra-deep visible images and additional near infrared photometry, that the cluster is there and that it is at a large redshift.

Ultra-deep visible and K band images might also reveal the position and the shape of the light distribution of the lensing galaxy. Such information would be useful to improve the mapping of the CO source, as already emphasised by Yun et al. (1997) and Alloin et al. (1997). With the present-day data, the CO source is found to be a ring-like structure with typical radius of ~ 100 pc, under the lens model of a galaxy and a cluster at $z=1.7$, leading to a central $\sim 10^9 M_\odot$ object, typical of a black-hole. It is

amazing to see that a disk with such a small intrinsic size can be spatially “resolved” even at a distance as large as $1.6 h_{50}^{-1}$ Gpc. However, we are aware that the CO source could have a more complex geometry and as long as the exact redshift and mass distribution of the lenses will not be known in a direct way, uncertainties on the CO source size will persist.

Although this remains to be confirmed independently, the discovery of a distant cluster of galaxies on the line of sight to the Cloverleaf is remarkable because it reinforces the suspicion that many bright high redshift quasars are magnified by cluster-like systems at large distances. This was already reported from analyses in the fields of the doubly imaged quasar Q2345+007 (Bonnet et al 1993; Mellier et al 1994; van Waerbeke et al 1997), where a cluster candidate is expected to be at $z \sim 0.75$ (Pelló et al 1996) and of MG2016 where the X-ray emission of the intra-cluster gas has been observed and for which the Iron line (from X-ray spectroscopy) gives a redshift $z \sim 1$ (Hattori et al 1997).

These cases of strong lensing may change substantially the intrinsic bright-end luminosity function of quasars. In fact, there is now convincing evidence that magnification biases play an important role and this should draw some important cosmological issues. Early observational evidence was emphasized by the galaxy-quasar associations detected by Fugmann et al (1990). They have been re-investigated and confirmed by Bartelmann & Schneider (1994) and Beñítez & Martínez-Gonzalez (1996). According to Bartelmann & Schneider (1992) the galaxy-quasar association on arcminute scale cannot be explained by lensing effects from single galaxies only, but must involve lensing effects by large-scale structure or rich cluster of galaxies. Since all these sources, including the Cloverleaf, are very bright, they correspond to preferentially selected fields which probe the bright-end of the magnified areas where we expect that the lensing agent responsible for magnification must be strong. If it is so, many bright quasars are magnified by massive gravitational systems. It would therefore be important to collect ultra-deep visible and near infrared high-resolution imaging on a large sample of overbright quasars in order to compute which fraction is surrounded by high-redshift foreground clusters of galaxies.

Though these fields correspond to biased lines of sight, they are typical fields showing the strong-end of cosmic shear event expected on arcminute scales from the predictions of Jain & Seljak (1996). By using the non-linear evolution of the power spectrum, these authors have shown that the rms cosmic shear on such scales is more than twice the values predicted from the weakly non-linear regime. Arguing that the cosmic shear should therefore be observable even with present-day ground based telescopes, Schneider et al (1997) have re-analysed the Fort et al (1996) data and have shown that the cosmic shear may have already been detected in at least one quasar field

(PKS1508). Very deep observations of the Cloverleaf, to confirm that a shear pattern with significant shear amplitude of order of 5% is present around the four spots, would provide independent data in favor of this interpretation.

The observation of cosmic shear or the detection of distant clusters put strong constraints on the density parameter Ω and on the initial power spectrum of density fluctuations. If most of the bright quasars are magnified by high-redshift clusters, then the density of distant clusters of galaxies must be large (this may conflict with the standard CDM model for example). However, the impact on cosmological scenarios is not clear since we do not understand yet the selection biases.

Though our multiwavelength analysis, using the best visible and CO images, provides a new interpretation of the Cloverleaf and a good understanding of the lens configuration, the discussion raises new questions about the CO source and the lenses. In order to address these questions thoroughly, additional photometric and spectroscopic data are required. Since the members of the cluster are extremely faint their spectroscopy and the measurement of the cluster velocity dispersion will be technically difficult. In addition to ultra-deep visible and near infrared imaging to probe the light distribution of the lenses (individual galaxy and cluster), the mass model representing the cluster could be considerably improved by using the shear pattern generated by the lensed background sources and from the redshift measurements of the ‘brightest’ cluster members. Last but not least, the photometric monitoring of the four spots (Østensen et al 1997) will provide the time delay of the light curves which is also an important and independent constraint for the modelling.

Acknowledgements. We thank M.-C. Angonin and C. Vanderriest for providing their CFHT images. We thank J. Bézecourt, S. Charlot, J.-M. Miralles and R. Pelló, for useful discussions and their help in using and interpreting properly the Bruzual & Charlot’ galaxy evolution models. We thank A. Lannes for useful discussion on deconvolution and inversion techniques, and J. Hjorth on multiple quasar lensing and PSF subtraction. DA and YM thank Observatoire Midi-Pyrénées for hospitality. We are grateful to CEA, CFHT, IRAM, ST-ECF and CADC for financial and technical supports.

References

- Alloin, D., Guilloteau, S., Barvainis, R., Antonucci, R., Tacconi, L. 1997, A&A, in press.
- Angonin, M.-C., Remy, M., Surdej, J., Vanderriest, C. 1990, A&A 233, L5.
- Arnould, P., Remy, M., Gosset, E. et al 1993, in “*Gravitational Lenses in the Universe*”, eds. J. Surdej et al., Université de Liège, p. 169.
- Bartelmann, M., Schneider, P. 1992, A&A 259, 413.
- Bartelmann, M., Schneider, P. 1994, A&A 284, 1.
- Barvainis, R., Tacconi, R., Antonucci, R., Alloin, D., Coleman, P. 1994, Nature 371, 586.

Barvainis, R., Maloney, P., Antonucci, R., Alloin, D. 1997, ApJ in press. Preprint astro-ph/9702118.

Benítez, N. & Martínez-González, E. 1996, astro-ph/9609183.

Bertin, E., Arnouts, S. 1996, A&AS 117, 393.

Bica, E., Alloin, D., Schmidt, A., 1990, MNRAS, 242, 241.

Bonnet, H., Fort, B., Kneib, J.-P., Mellier, Y., Soucail, G. 1993, A&A 280, L7.

Bruzual, G., Charlot, S. 1993, ApJ 405, 538.

Falco, E. E. 1993, in "Gravitational Lenses in the Universe", eds. J. Surdej et al., Université de Liège, p. 127.

Fall, S., M. 1981, in "The Structure and Evolution of Normal Galaxy", eds. S. M. Fall and D. Lynden-Bell. Cambridge University Press, p. 1.

Fort, B., Mellier, Y., Dantel-Fort, M., Bonnet, H. & Kneib, J.-P. 1996, A&A 310, 705.

Fugmann, W. 1990, A&A 240, 11.

Hattori et al 1997, Nature, in press.

Hjorth, J., Kneib, J.-P. 1997, preprint.

Hjorth, J., Madsen, J. 1995, ApJ 445, 55.

Jain, B., Seljak, U. 1996. Preprint astro-ph/9611077.

Kassiola, A., Kovner, I. 1993, ApJ 417, 450.

Kayser, R., Surdej, J., Condon, J., Kellermann K. I., Magain, P., Remy, M., Smette, A. 1990, ApJ 364, 15.

Kneib, J.-P., Mellier, Y., Fort, B., Mathez, G. 1993, A&A 273, 370.

Kneib, J.-P., Ellis, R. S., Smail, I., Couch, W. J., Sharples, R. M. 1996, ApJ 471, 643.

Lawrence, C. R. 1996, in "Astrophysical Applications of Gravitational Lensing", eds. C. Kochanek & J. Hewitt, Kluwer, p. 209.

Lilly, S.J., Hammer, F., Le Fèvre, O., Crampton, D., 1995, ApJ 455, 75.

Magain, P., Surdej, J., Swing, J.-P., Borgeest, U., Kayser, R., Kühr, H., Refsdal, S., Remy, M. 1988, Nature 334, 325.

Mellier, Y., Dantel-Fort, M., Fort, B., Bonnet, H. 1994, A&A 289, L15.

Østensen, R., Remy, M., Lindblad, P. O., Refsdal, S., Stabell, R., Surdej, J., Barthel, P. D., Emanuelson, P. I., Festin, L., Gosset, E., Hainaut, O., Hakala, P., Hjelm, M., Hjorth, J., Hutsemékers, D., Jablonski, M., Kaas, A. A., Kristen, H., Larsson, S., Magain, P., Pettersson, B., Pospieszalska, Surdej, A., Smette, A., Teuber, J., Thomsen, B., Van drom, E. 1997, A&AS in press.

Pelló, R., Miralles, J.-M., Le Borgne, J.-F., Picat, J.-P., Soucail, G., Bruzual, G. 1996, A&A 314, 73.

Schneider, P., Van Waerbeke, L., Mellier, Y., Jain, B., Seitz, S., Fort, B. 1997. Preprint astro-ph/9705122.

Van Waerbeke, L., Mellier, Y., Schneider, P., Fort, B. & Mathez, G. 1997, A&A 317, 303.

Wilner, D. J., Zhao, J.-H., Ho, P. T. 1995, 453, L91.

Telles, E., Terlevich, R., 1997, MNRAS 286, 183.

Turnshek, D.A., Foltz, C.B., Grillmair, C.J., Weyman, R.J., 1988, ApJ, 325, 651

Turnshek, D.A., 1995 in "ESO Astrophysics Symposium" Garching 21-24 Nov. 94, ed. G. Meylan, p. 223. Springer-Verlag.

Yun, M. S., Scoville, N. Z., Carrasco, J. J., Blandford, R. D. 1997, ApJ 479, L9

This figure "fig1.gif" is available in "gif" format from:

<http://arxiv.org/ps/astro-ph/9706036v1>

This figure "fig4.gif" is available in "gif" format from:

<http://arxiv.org/ps/astro-ph/9706036v1>

This figure "fig5.gif" is available in "gif" format from:

<http://arxiv.org/ps/astro-ph/9706036v1>

This figure "fig6.gif" is available in "gif" format from:

<http://arxiv.org/ps/astro-ph/9706036v1>